

# Kinematic Optimization of Energy Extraction Efficiency for Flapping Airfoil by using Response Surface Method and Genetic Algorithm

M. Maatar<sup>1†</sup>, M. Mekadem<sup>2</sup>, M. Medale<sup>3</sup> and B. Imine<sup>4</sup>

<sup>1</sup>Aeronautics and Propulsive Systems Laboratory, Faculty of Mechanical Engineering, Department of Mechanics, University of Sciences and Technology of Oran Mohamed Boudiaf, BP. 1505 Oran El M'Naouer, 31000 Oran, Algeria

<sup>2</sup>LMF, Ecole Militaire Polytechnique (EMP), B.P 17 Bordj-el-Bahri, 16111, Algiers, Algeria

<sup>3</sup>IUSTI Laboratory, UMR 7343 CNRS-University of Aix-Marseille Technopole de Chateau-Gombert, 5 rue Enrico Fermi 13453 MARSEILLE, Cedex 13, France

<sup>4</sup>Aeronautics and Propulsive Systems Laboratory, Faculty of Mechanical Engineering, Department of Mechanics, University of Sciences and Technology of Oran Mohamed Boudiaf, BP. 1505 Oran El M'Naouer, 31000 Oran, Algeria

†Corresponding Author Email: [mounir.maatar@univ-usto.dz](mailto:mounir.maatar@univ-usto.dz)

(Received November 10, 2022; accepted January 20, 2023)

## ABSTRACT

In this paper, numerical simulations have been performed to study the performance of a single fully activated flapping wing serving as energy harvester. The aims of the paper are predicting and maximizing the energy extraction efficiency by using optimization methodology. The metamodeling and the genetic algorithms are applied in order to find the optimal configuration improving the efficiency. A response surface method (RSM) based on Box–Behnken experimental design and genetic algorithm has been chosen to solve this problem. Three optimization factors have been manipulated, i.e. the dimensionless heaving amplitude  $h_0$ , the pitching amplitude  $\theta_0$  and the flapping frequency  $f$ . The ANSYS FLUENT 14 commercial software has been used to compute the governing flow equations at a Reynolds number of 1100, while the flapping movement combined from heaving and pitching of the NACA0015 foil has been carried out by using an in house user-defined function (UDF). A maximum predicted efficiency of 34.02% has been obtained with high accuracy of optimal kinematic factors of dimensionless heaving amplitude around the chord, high pitching amplitude and low flapping frequency of 0.304 hertz. Results have also showed that the interaction effect between optimization factors is important and the quadratic effect of the frequency is strong confirming the great potential of the applied optimization methodology.

**Keywords:** Numerical simulation; Flapping wing; Energy extraction; Efficiency; Box–Behnken.

## NOMENCLATURE

$c$	foil chord length	$\phi$	phase angle between heaving and pitching motions
$Cop$	instantaneous power coefficient	$f$	flapping frequency
$Coph$	heave motion instantaneous power coefficient	$F_Y(t)$	instantaneous vertical force
$Coph\text{-mean}$	time-averaged power coefficient of heaving motion	$h_0$	dimensionless heaving amplitude
$Cop\theta$	pitch motion instantaneous power coefficient	$h(t)$	heaving motion
$Cop\theta\text{-mean}$	time-averaged power coefficient of pitching motion	$M_z(t)$	instantaneous moment
$Cop\text{mean}$	time-averaged power coefficient	$P$	instantaneous total power extracted
$C_p$	pressure coefficient	$P_a$	total power available in flow
$C_M$	moment coefficient	$RMSE$	Root Mean Squared Error
$C_Y$	lift coefficient	$R^2$	coefficient of determination
$dh/dt$	heaving velocity	$R_e$	Reynolds number
		$St$	Strouhal number
		$T$	flapping period ( $T = 1/f$ )
		$t$	physical time

$d\theta/dt$	pitching angular velocity	$U_\infty$	free stream velocity
$d$	maximum vertical displacement of the trailing edge	$V_{eff}$	effective upstream velocity
$E_r$	relative error	$x_p$	chordwise position of pitching axis
$\theta_0$	pitching amplitude	$\alpha_{eff}$	effective angle of attack
$\theta(t)$	pitching motion	$\eta$	energy extraction efficiency
		$\chi$	feathering parameter

## 1. INTRODUCTION

Humanity's need for energy is constantly increasing, due to its consumption in all life aspects (Xu *et al.* 2021). This dependence has pushed researchers to look for new renewable energy sources. This type of energies are becoming more and more beneficial, considering their advantages such as, reducing the negative impacts on the environment, decreasing the extracted energy's cost, exploiting a new energy sources and eliminating the problem of waste storage (Ma *et al.* 2018). Oscillating wings are the new concept used in extracting energy from incoming winds and water currents. This turbines type guarantees low depth of the fluid involved (rivers), low operating speeds, reduced noise, small wings and a competitive efficiency with the one obtained by rotary turbines. Moreover the oscillating wings have gradually become a focus of numerical and experimental investigations in the last decade (Zhu *et al.* 2018). Evaluating the energy extraction performances by simulation is a computationally expensive task that requires powerful computing resources. The use of optimization has become an indispensable tool to acquire a good prediction of performances at inexpensive numerical cost.

The first oscillating wing harvester system in the literature has been attributed to McKinney and DeLaurier (1980), who have investigated the feasibility of energy extraction by using mechanical mechanism from the wind by means of an oscillating wing performing a combined heave and pitch motion. The maximum efficiency obtained by this mechanism has reached 17%. This increase is mainly due to the principal contribution of lift forces in the extracted energy. Using flapping wings as wind and water turbines has been studied by performing 2D Navier-Stokes computations (Platzer *et al.* 2009). The results indicate that the adoption of non-sinusoidal flapping motion increases the energy extraction performance by 30% compared to wings adopting a sinusoidal flapping motion. A numerical study of a two-dimensional laminar flow of an oscillating wing set in heaving and pitching motion has been realized (Kinsey and Dumas 2008). An energy extraction efficiency that exceeds 35% has been achieved with a heaving amplitude of chord's order, a reduced frequency of 0.15 and a pitching amplitude greater than 75 degrees. The wing can achieve a maximum effective attack angle equal 35 degrees. The effect of non-sinusoidal motion trajectory on the energy extraction performances namely, the extracted power and the efficiency have been investigated (Xiao *et al.* 2012). A trapezoidal motion trajectory coupled with a sinusoidal heaving motion has been adopted. The study results reveal that the prescribed motion configuration

significantly increases the extracted power from the fluid and the efficiency is respectively up to 63% and 50%. Zhu and Tian (2017) have numerically examined the asymmetric time effect of pitching motion on energy extraction performance of a flapping wing designed as energy harvester. The adopting asymmetric time of pitching motion under certain optimal parameters increases the energy extraction efficiency of the flapping wing, up to 17% compared with the time symmetric pitching motion of flapping wing energy harvester. With the aim to maximize the energy extraction performance from a flapping wing at a reduced numerical simulation cost, evolutionary algorithms are used (Liu *et al.* 2018). The multi-fidelity evolutionary algorithm strategy proves to be more methodical for the prediction of kinematic motion parameters maximizing the energy extraction efficiency and/or the averaged power coefficient. A numerical and experimental study has been performed (Zhu 2019). The use of deformable wings has been studied in order to understand the physical phenomena of the flow around a deformable flapping wing that lead to increasing the energy extraction performance. A maximum efficiency is achieved when the position of deformation center is superimposed on the position of the flapping wing pivot point.

Zheng *et al.* (2020a) reported that the optimal kinematic configuration parameters of the flapping airfoil can be efficiently detected with specific aerodynamic performance using the multifidelity Gaussian process regression and Bayesian optimization. Li *et al.* (2022) have indicated that the aerodynamic characteristics and the physical fields of a flapping wing energy harvester are predicted with accuracy at a minimum computational cost by using deep learning based on real-time model founded in two modular convolutional neural networks. Zheng *et al.* (2020b) have carried out a framework optimization method created on the data-informed self-adaptive quasi-steady model. The kinematic parameters of the flapping ellipsoid wing have been optimized in order to predict the optimal time-averaged lift coefficient. Ji *et al.* (2022) have also indicated that the enhancement of thrust and propulsive efficiency of a tandem flapping wings is rapidly reached by using the multi-fidelity Gaussian process regression and Bayesian optimization detecting the optimal kinematic parameters of wings flapping motion. The optimal parameters that lead to maximizing the efficiency of a mixed biodiesel comprising two substances, namely J. curcas and C. pentandra by using the response surface method, have been studied (Dharma *et al.* 2016). The biodiesel production process is passed by two phases. The first one contains an acid catalyzed esterification followed by an alkali catalyzed transesterification, and this method has been applied

based on the Box-Behnken design of experiment led to find the optimal configuration of the optimization parameters that gives an efficiency of 93.33%. In order to determine the prediction efficiency of the acid value in PKO acid pretreatment, [Betiku \*et al.\* \(2016\)](#) have utilized response surface methodology (RSM), ANFIS and ANN. The results point out how necessary is using optimization methods in PKO acid pretreatment in order to find the optimal configuration of optimization variables reducing the oil acid value. It is worth mentioning that the ANFIS and ANN methods show higher and more accurate prediction efficiency, but following RMS method is sufficient if it allows evaluating the interaction between the optimization variables.

In present work, an attempt to study a flapping foil performance has been made by relying on 2-D numerical simulation. We are particularly interested in using optimisation methodology to predict and maximize energy extraction efficiency of a NACA 0015 by using it as a single fully activated flapping wing. However, in order to identify the optimal configuration of kinematic parameters; metamodeling and genetic algorithms are applied. In order to solve this problem, a response surface approach based on Box-Behnken experimental design and a genetic algorithm has been selected. At a low Reynolds number, the commercially available software ANSYS FLUENT 14 has been used to solve the governing flow equations. The dimensionless heaving amplitude, the pitching amplitude, and the flapping frequency have been all adjusted during the optimization process.

## 2. FLAPPING WING KINEMATIC

Conventionally, a flapping wing is a wing that simultaneously performs a heave and pitch motion. The heave is the vertical wing displacement and the pitch is the wing rotation around a pivot point localized at  $x_p$  distance from the leading edge, as shown in Fig. 1, while the flapping motion is imposed according to a sinusoidal trajectories. For that the heaving motion is given by:

$$h(t) = ch_0 \sin(2\pi ft) \quad (1)$$

The pitching motion is carried out around a pivot point located at one third of the chord from the leading edge, where the foil chord is  $c=100$  mm. The pitching motion is released according to the following formula.

$$\theta(t) = \theta_0 \sin(2\pi ft + \phi) \quad (2)$$

Where,  $h_0$  is the dimensionless heaving amplitude;  $\theta_0$  is the pitching amplitude;  $\phi$  is the phase angle between the pitching and heaving motions and finally  $f$  is the flapping frequency.

The Strouhal number that considers the temporal spatial effect is used to characterize the energy extraction efficiency. According to [Anderson \*et al.\* \(1998\)](#) the Strouhal number is defined as follows:

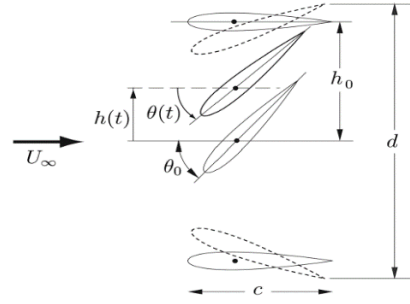


**Fig. 1. Movement of the flapping wing (Kinsey and Dumas 2008).**

$$St = fd/U_\infty \quad (3)$$

Where  $d$  represents the maximum vertical displacement of the trailing edge given by the following expression:

$$d = ch_0 + 2(c - x_p) \sin \theta(t) \quad (4)$$

Where  $x_p$  represent the chordwise position of pitching axis.

The vertical displacement of the wing in the flow induces an effective angle of attack  $\alpha_{eff}$  and an effective upstream velocity  $V_{eff}$ , expressed according to ([Kinsey and Dumas 2008](#)) as follows:

$$\alpha_{eff} = \arctan\left(-\frac{dh/dt}{U_\infty}\right) - \theta(t) \quad (5)$$

$$V_{eff} = \sqrt{U_\infty^2 + (dh(t)/dt)^2} \quad (6)$$

The maximum values of  $\alpha_{eff}$  and  $V_{eff}$  over a flapping period have significant effects on the aerodynamic forces and on the possibility of dynamic-stall occurrence.

The operating regime of flapping wings is determined according to the value of feathering parameter  $\chi$  ([Anderson \*et al.\* 1998](#)), propulsion if ( $\chi < 1$ ) or energy extraction if ( $\chi > 1$ ). The feathering parameter is given by the following formula:

$$\chi = \frac{\theta_0}{\arctan(ch_0 w / U_\infty)} \quad (7)$$

In the energy extraction operating regimes, the vertical component of the resulting aerodynamic force is in the same direction as the vertical displacement of the wing ([Kinsey and Dumas 2008](#)).

## 3. PERFORMANCE OF ENERGY EXTRACTION

The instantaneous extracted power in a flapping cycle is the summation of that extracted from the heave and pitch motion, as it is expressed. The instantaneous power coefficient is equal to:

$$C_{op} = \frac{P}{0.5\rho U_{\infty}^3 c} \quad (8)$$

Otherwise, it is expressed like:

$$C_{op} = \frac{C_Y(t)}{U_{\infty}} \frac{dh(t)}{dt} + \frac{C_M(t)}{U_{\infty}} \frac{d\theta(t)}{dt} = C_{op_h} + C_{op_{\theta}} \quad (9)$$

Where the lift and the moment coefficients  $C_Y$  and  $C_M$  are given respectively by:

$$C_Y(t) = \frac{F_Y(t)}{1/2\rho U_{\infty}^2 S} \quad (10)$$

$$C_M(t) = \frac{M_z(t)}{1/2\rho U_{\infty}^2 S} \quad (11)$$

The average mean power during one cycle is given by:

$$\bar{P} = \frac{1}{T} \int_0^T P dt \quad (12)$$

While the mean power coefficient is expressed with the following formula:

$$C_{op_{mean}} = \frac{\bar{P}}{0.5\rho U_{\infty}^3 c} \quad (13)$$

The energy extraction efficiency is defined as:

$$\eta = \frac{\bar{P}}{P_a} = C_{op_{mean}} \frac{c}{d} \quad (14)$$

Where, the total power available in flow  $P_a$  is expressed as follows:

$$P_a = \frac{1}{2} \rho U_{\infty}^3 d \quad (15)$$

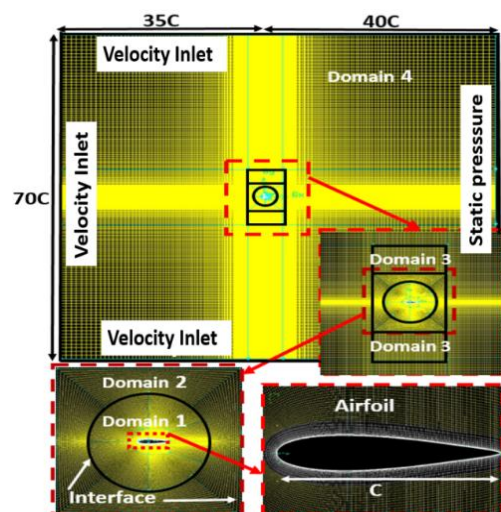


Fig. 2. Meshing strategy adopted in the present study.

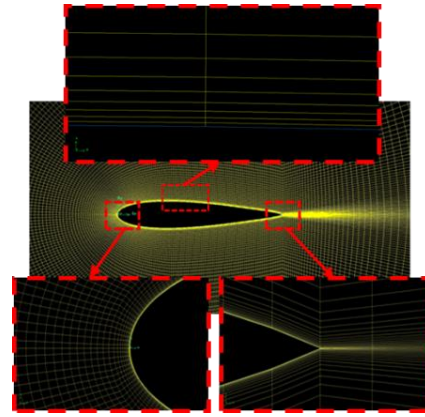


Fig. 3. Zoom of the mesh around the profile.

## 4. NUMERICAL APPROACH

### 4.1 Grid Generation

Geometry model and mesh generation are created with GAMBIT software. The computational domain inlet and outlet from the profile leading edge, as represented in Fig. 2, are localized respectively at 35c and 40c. The upper and the bottom far fields are located at 35c. The structured mesh has been used and the computational domain has been divided into four subdomains in order to control separately each mesh part. The first one rotates around the pivot point  $x_p$  and moves up and down with the second subdomain. The third one has been kept stationary with deforming meshes and the fourth domain has been stationary.

Figure 3 also shows a zoom of the mesh around the profile, the leading edge and the trailing edge where the thickness of the first layer is 0.0015m.

### 4.2 Flow Solver

The simulations are conducted with the ANSYS FLUENT 14 software for two-dimensional, unsteady flow with laminar flow conditions assumed according to (Kinsey and Dumas 2008; Xiao *et al.* 2012; Boudis *et al.* 2021). A solver based on the pressure is used to solve the Navier-Stokes equations around the airfoil with a velocity-pressure coupling SIMPLE algorithm. For the space discretization, the third order MUSCL scheme is used for the advective terms meanwhile one uses a first order temporal discretization, imposed by the dynamic mesh used. The flapping motion is ensured by the Dynamic Layering method available in ANSYS FLUENT 14 that requires the introduction of a function defined by the user (UDF). The elaborated UDF is also applied to calculate the aerodynamic coefficients, the energy extraction performances, and to control the airfoil kinematic parameters of flapping motion.

The boundary conditions are:

1. Inlet velocity at inlet, upper and bottom;
2. Outlet static pressure at domain outlet;
3. Wall with no slip velocity on the airfoil.

The numerical computations are conducted in a workstation running on Linux operating system with CPU Intel(R) Xeon(R) E5-2620 v4 2.10 GHz, and 32 Gb memory. The Navier-Stokes solver and the optimization software are compiled by using ANSYS FLUENT 14 and MATLAB, where the computational cost of one simulation with 8 periods would be 6 hours.

## 5. OPTIMIZATION METHODS

The mathematical formulation of an optimization problem according to [Haftka \(1996\)](#) is given as follows:

$$\begin{cases} \text{Min}(Y(x)) \\ x = (x_1, x_2, x_3, \dots, x_k) \\ x_{\min} < x < x_{\max} \end{cases} \quad (16)$$

The adopted optimisation approach is divided in two stages. The first one uses the metamodeling to approximate the objective function  $Y(x)$  that is unknown (evaluated by simulation) and the second stage relies on the application of an optimization method in order to maximize the predicted objective function.

### 5.1. Approximation of the Objective Function by RSM

This method's principle consists in replacing the actual(observed) function  $Y(x)$  which is evaluated by experiments (simulation), by an explicit approximated function  $\hat{Y}(x)$  according to the optimization variables  $(x_1, x_2, x_3, \dots, x_k)$ . The function  $\hat{Y}$  is determined from the preliminary calculation of the  $Y(x)$  function for a limited number of simulations selected in accordance with a design experiment ([Myers et al. 2004](#)).

The quadratic polynomial approximation is used because it is the most popular form due to its flexibility when approximating nonlinear response according to [Box and Behnken \(1960\)](#). A quadratic polynomial RSM with  $k$  variables can be written as follows:

$$Y = \beta_0 + \sum_{i=1}^k \beta_i x_i + \sum_{i=1}^k \beta_{ii} x_i^2 + \sum_{i=1}^{k-1} \sum_{j=i+1}^k \beta_{ij} x_i x_j + \varepsilon \quad (17)$$

Where:  $x_i$  and  $x_j$  represent the optimization variables (also called factors) and  $\beta_i, \beta_{ii}, \beta_{ij}$  are the polynomial coefficients to be determined,  $\varepsilon$  represents the error between the modelled values and the observed (simulated) values. The multilinear regression technique is employed to identify the values of the coefficients ( $\beta_i, \beta_{ii}, \beta_{ij}$ ) that minimize the least squares criterion on the errors ([Park and Dang 2010](#)).

### 5.1.1. Box-Behnken Based Experimental Design

An experimental design based on the Box-Behnken has been selected according to the response surface construction. This choice is justified by the good adaptation of this design type to the polynomial approximation and also by the number of the reduced simulation which requires this design experiment. The necessary experiments number ( $N$ ) is calculated by  $N=2k(k-1) + C_0$ , where  $k$  is the factors number and  $C_0$  is the number of central point's ([Shukla and Nishkam 2014](#)).

### 5.1.2. Validation of the Response surface method

Once the mathematical models are obtained, it is necessary to verify whether these models give an adequate approximation of the studied physical phenomenon ([Park and Dang 2010](#)). For this, the calculation of the following errors (statistical estimator) is considered. Mean absolute error, root mean squared error (RMSE), and coefficient of determination  $R^2$ , are respectively given by Eqs. (18), (19) and (20).

$$E_{AM} = \frac{\sum_{i=1}^n (Y_i - \hat{Y}_i)}{n} \quad (18)$$

$$RMSE = \sqrt{\frac{\sum_{i=1}^n (Y_i - \hat{Y}_i)^2}{n}} \quad (19)$$

$$R^2 = 1 - \frac{\sum_{i=1}^n (Y_i - \hat{Y}_i)^2}{\sum_{i=1}^n (Y_i - \bar{Y})^2} \quad (20)$$

Where  $Y_i, \bar{Y}_i$  and  $\hat{Y}(x)$  are, respectively, the observed values, the mean of the observed values and the approximated (predicted) values.

## 5.2 Maximization of Objective Function using GA

After obtaining the approximate objective function  $\hat{Y}(x)$ , an implementation of an optimization method is necessary, in order to determine the optimum of the approximate objective function in the chosen search intervals. For this, genetic algorithms (GAs), are used. They have been initially developed by [Holland \(1992\)](#) and popularized by [Goldberg \(2000\)](#). The selection of the mentioned method is justified by the genetic algorithms performance that avoids local minima.

## 6. Results and Discussion

### 6.1 Numerical Approach Validation

The validation of the adopted numerical approach is performed against the work of [Kinsey and Dumas \(2008\)](#).

**Table 1 Data of, Drag coefficient, mean power coefficient and efficiency for height periods**

Periods	$\bar{C}_x$	$Cop_{mean}$	$\eta$	$E_r(\bar{C}_x)\%$	$E_r(Cop_{mean})\%$	$E_r(\eta)\%$
2	-2,060	0,907	0,354	-3,362	-4,133	-4,118
3	-1,993	0,871	0,34	-0,911	-1,044	-1,190
4	-1,975	0,862	0,336	-0,407	-0,466	-0,299
5	-1,967	0,858	0,335	-0,153	-0,234	-0,299
6	-1,964	0,856	0,334	-0,255	-0,352	-0,300
7	-1,959	0,853	0,333	-0,051	-0,117	0,000
8	-1,960	0,854	0,333	-0,102	-0,117	0,000

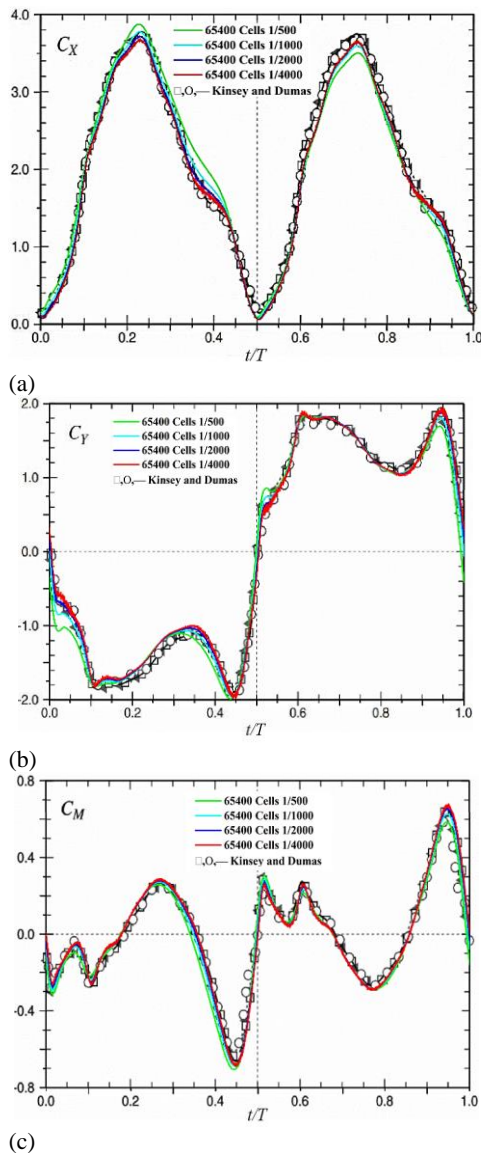


**Fig. 4. Force coefficients comparison between reference and the present study, (a) drag coefficient, (b) lift coefficient and (c) moment coefficient, as function of time step.**

Therefore numerical simulations are conducted at a Reynolds number of 1100, a reduced frequency  $f^*=0.14$ ,  $\theta_0=76.33^\circ$ ,  $h_0=1$ ,  $x_p=0.33c$  and  $\phi=90^\circ$ . The validation is performed through quantitative comparisons of the averaged drag coefficient  $\bar{C}_x$ , the mean power coefficient  $Cop_{mean}$  and the efficiency  $\eta$ . The results obtained from the eighth period have

been selected where the relative error between two consecutive coefficients periods becomes less than 0.1 %, as shown in Table 1.

Another validation of the numerical approach is performed through quantitative comparisons of the force coefficients (drag, lift, and moment) over one period.

The results of the force coefficients are compared with those of the reference through a spatial and temporal discretization in Figs. 4. (a), (b) and (c) and Figs. 5. (a), (b) and (c).

The concluded results from the eight period have been chosen where the relative error  $E_r$  of the average force becomes negligible between two consecutive periods.

### 6.1.1 Temporal Discretization

Four time steps have been picked in order to study the stability of the numerical solution regarding the temporal discretization. The time steps used are 1/500, 1/1000, 1/2000, and 1/4000 with a mesh size of 65400 cells.

What is remarkable is that from a time step of 1/2000 the curves of the force coefficients are perfectly close to those of Kinsey and Dumas (2008).

After going through a spatial and temporal discretization, a mesh with 65400 cells and a time step of 1/2000 have been adopted in order to have a quality numerical solution with an acceptable computation cost and the adopted mesh will be used for subsequent research.

The followed numerical approach is validated against the literature as shown in Figs. 6 and it can reproduce the physical phenomena listed in the literature.

## 6.2 Prediction and Maximization of the Efficiency

This study aims at finding the optimal configuration of flapping airfoil kinematic parameters (dimensionless heaving amplitude, pitching amplitude, and flapping frequency) that maximize the efficiency where the search intervals for optimization factors are fixed from the study of Kinsey and Dumas (2008).

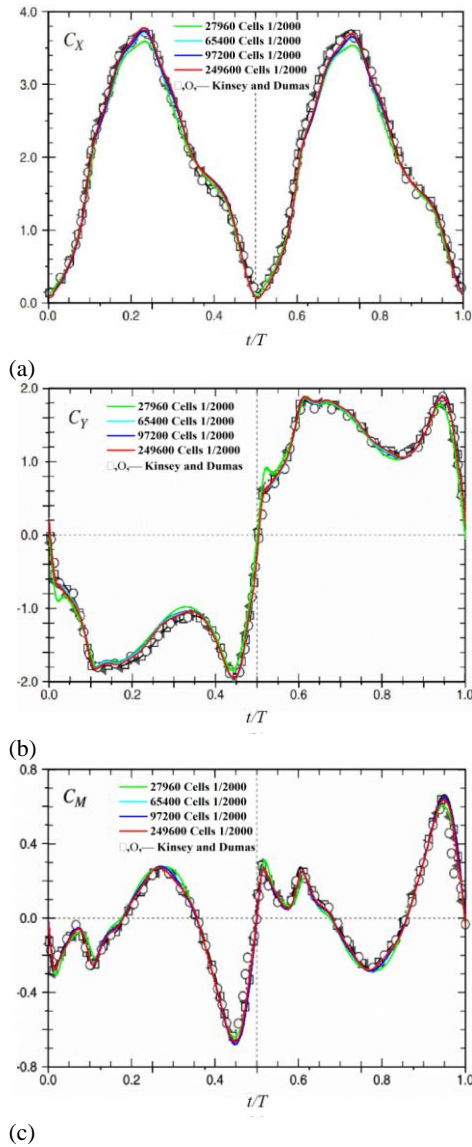


**Fig. 5. Force coefficients comparison between reference and the present study, (a) drag coefficient, (b) lift coefficient and (c) moment coefficient, as function of cells number.**

According to Eq. (16), the optimization problem in this study is given as follows:

$$\begin{cases} \text{Min}(\eta(x)) \\ x = (h_0, \theta_0, f) \\ 0.7 \leq h_0 \leq 1.3 \\ 1.33(76^\circ) \leq \theta_0 \leq 1.5(86^\circ) \\ 0.25 \leq f \leq 0.35 \end{cases} \quad (21)$$

### 6.2.1 Response Surface Approximation

In this work, the necessary simulation number to create the Box-Behnken response surface with three factors  $h_0$ ,  $\theta_0$  and  $f$  is 15 where the three simulations are in the center points. The surface is constructed through the 13 responses (efficiency) of the

simulations that are carried out by the ANSYS FLUENT 14 software, with the simulation parameters  $h_0$ ,  $\theta_0$  and  $f$  set for each simulation in order to obtain the responses  $\eta$ .

The quadratic polynomial approximation of the efficiency as a function for the optimization factors  $h_0$ ,  $\theta_0$  and  $f$  is written as follows:

$$\begin{aligned} \hat{\eta}(h_0, \theta_0, f) = & \beta_1 + \beta_2 h_0 + \beta_3 \theta_0 + \beta_4 f + \\ & \beta_5 h_0^2 + \beta_6 h_0 \theta_0 + \beta_7 h_0 f + \beta_8 \theta_0^2 + \\ & \beta_9 \theta_0 f + \beta_{10} f^2 \end{aligned} \quad (22)$$

After determining  $\beta_i$  coefficient using the least squares minimization of the error between the response surface and the efficiency values are

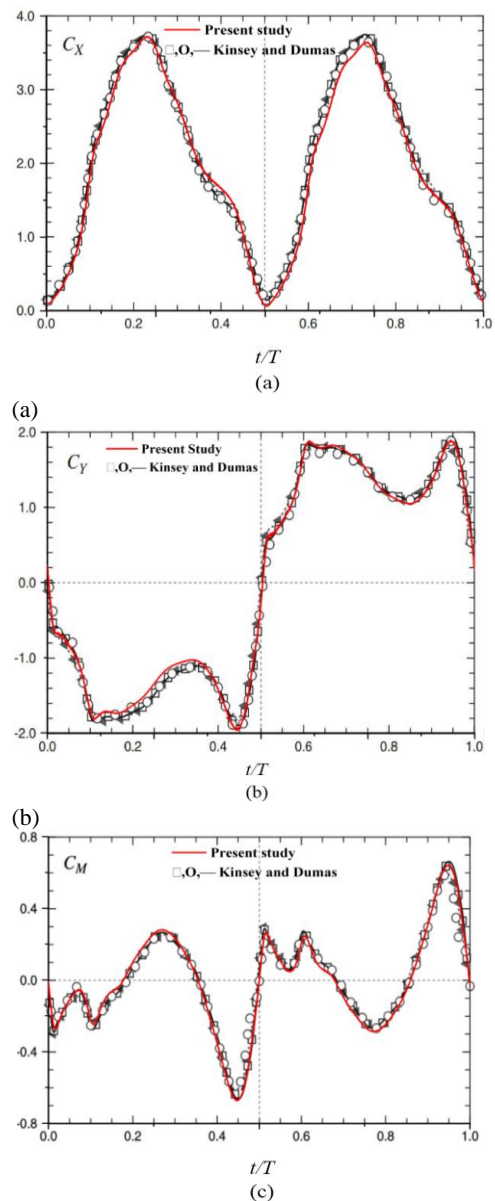


**Fig. 6. Force coefficients validation, (a) drag coefficient, (b) lift coefficient and (c) moment coefficient.**

obtained from the 13 simulations based on the Box-Behnken experimental design. By injecting the calculated values of  $\beta_i$  in Eq. (22), the approximated polynomial efficiency takes the following form:

$$\hat{\eta}(h_0, \theta_0, f) = -0.881 - 0.296h_0 - 1.296\theta_0 + 2.991f - 0.16h_0^2 - 0.539h_0\theta_0 - 0.5h_0f - 0.813\theta_0^2 - 1.529\theta_0f - 7.65\beta_{10}f^2 \quad (23)$$

### 6.2.2 RMS Methodology Validation

The predicted efficiency credibility using RSM is measured through the calculated statistical estimators cited in section (5.1.2). The predicted values using the polynomial response surface constructed based on the Eq. (23) illustrate that the approximate efficiency is very close to the actual efficiency obtained by the simulation, confirmed with, a coefficient of determination  $R^2$  of 0.999, a Mean absolute error  $E_{AM}$  of  $8.86e-04$  and a root mean squared error RMSE of  $3.43e-03$ . The red line in Fig. 6 represents the predicted efficiency versus the actual efficiency based on the formula (Predicted\_efficiency=0.999\*Actual\_efficiency), the blue points are obtained by the actual efficiency and the efficiency is calculated by using the formula Eq. (23). Figure 6 demonstrates the prediction credibility by using RSM method. This adequate prediction quality is illustrated by the value of the coefficient of determination around the unit signifying the reliability of the RSM model.

### 6.2.3 Genetic Algorithms Optimization

Depending upon MATLAB optimization genetic algorithms, the problem in Eq. (21) has been solved with the following parameters, i.e. chromosome length of three, the population size of 100 individuals, maximum iteration number of the population regeneration process of 100, selection, crossover The mutation probabilities are set to  $P_s=0.5$ ,  $P_c=0.8$ , and  $P_m=0.02$  respectively. The probabilities  $P_s$  and  $P_c$  are modified based on the roulette selection method.

The problem resolution using metamodeling and

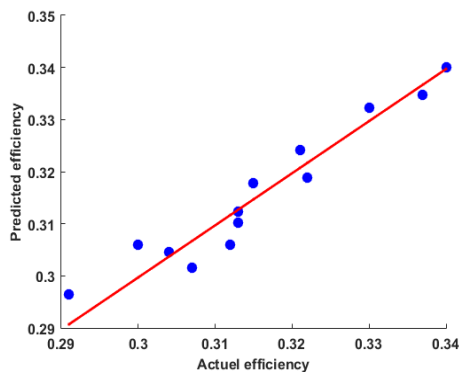


Fig. 7. Plot of the predicted efficiency given by RSM versus the actual efficiency.

genetic algorithms (MMGA) gives the following results of optimal predicted efficiency  $\hat{\eta}_{Optimal}$  of 0.3402, and the optimal configuration of the optimization factors is, a dimensionless heaving amplitude  $h_{0-Optimal}$  of 0.968, a pitching amplitude  $\theta_{0-Optimal}$  of 1.404 radian (80.44 degrees) and a flapping frequency  $f_{Optimal}$  of 0.304 hertz. The optimal predicted efficiency using MMGA is improved with respect to that observed in numerical validation cited in Table.1 by 2%.

### 6.2.4 Efficiency Derivatives at the Optimum

The partial derivative function of the polynomial efficiency approximation goes by:

$$d\hat{\eta}/dh_0 = \beta_2 + 2\beta_5h_0 + \beta_6\theta_0 + \beta_7f$$

$$d\hat{\eta}/d\theta_0 = \beta_3 + \beta_6h_0 + 2\beta_8\theta_0 + \beta_9f$$

$$d\hat{\eta}/df = \beta_4 + \beta_7h_0 + \beta_9\theta_0 + 2\beta_{10}f$$

The derivatives calculation at the optimum point is completed by injecting the optimal configuration values  $h_{0-Optimal}$ ,  $\theta_{0-Optimal}$  and  $f_{Optimal}$  into the following equations. The derivatives values at the optimum point are  $d\hat{\eta}/dh_0 = -5.479e-06$ ,  $d\hat{\eta}/d\theta_0 = 2.982e-06$  and  $d\hat{\eta}/df = -1.429e-04$ . The derivatives efficiency considering optimization factors at the optimum point is around zero, which confirms that the optimum found by MMGA is trustworthy.

### 6.2.5 Verifying Optimal Efficiency with Simulation

The optimal configuration of the dimensionless heaving amplitude  $h_{0-Optimal}$  of 0.968, pitching amplitude of 1.404 radian (80.44 degrees) and flapping frequency  $f_{Optimal}$  of 0.304 hertz have been checked by the simulation and the efficiency of 0.341 is reached out. These results show that the MMGA predicts the optimal efficiency with a relative error of 0.29% compared to the simulation which confirms that the given results by the MMGA are very close to those of the simulation, certifying the usefulness of the adopted MMGA methodology.

From Figs. 8, comparing the force coefficients of the simulated optimum obtained by the MMGA and those of Kinsey and Dumas (2008), it comes out that, the drag coefficient found by using the simulated optimum is quasi similar to that of the reference over most of the period, except around the instants 0.2T and 0.7T where the peaks of the drag coefficient using simulated MMGA configuration are the greatest, due to the high maximum values of  $\alpha_{eff}$  and  $V_{eff}$  of  $37.24^\circ$  and 0.27 m/s compared to those of the reference which are equal to  $34.37^\circ$  and 0.26 m/s respectively during the instants of 0.25T and 0.75T as shown in Figs. 9. In fact, the main properties of the flow (such as the presence and timing of LEVS) are observed to be different between the two cases as revealed from Figs. 12, given the increase in frequency and the maximum effective angle of attack for the simulated optimum.

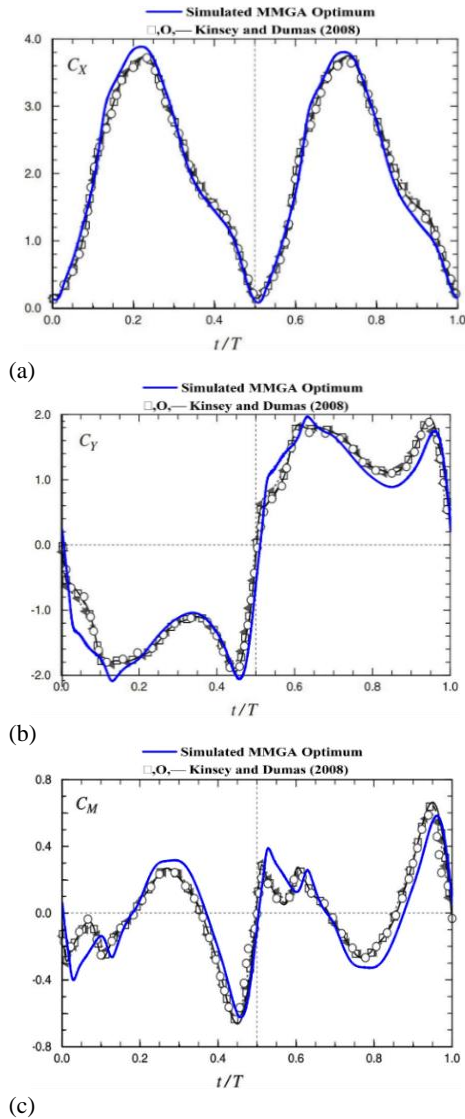


**Fig. 8. Force coefficients of, the simulated MMGA optimum and the reference, (a) drag coefficient, (b) lift coefficient and (c) moment coefficient.**

Concerning the lift coefficient of the simulated optimum depicted in Fig. 8(b), it is in good agreement with that of the reference during the period but not for the time instants  $0.1T$  and  $0.6T$  or near them where the lift coefficient and its peaks are improved for the simulated configuration. With respect to simulation results of the moment coefficient using simulated results of the optimum found by MMGA, plotted in Fig 8(c), it is remarkable that it is improved in the time intervals of  $0.025T$  to  $0.1T$ ,  $0.2T$  to  $0.35T$ ,  $0.5T$  to  $0.6T$ , and  $0.7T$  to  $0.875T$  and slightly decreased in the time intervals of  $0.35T$  to  $0.5T$  and  $0.85T$  to  $0.95T$  compared to that of the reference due to the growth in  $C_y$  in the cited time intervals.

The improvement of the efficiency using MMGA approach has been explained through the power coefficient according to the formula defined in Eq. (14). The comparison of the instantaneous power coefficient  $Cop_h$ ,  $Cop_\theta$  and  $Cop$  over a flapping

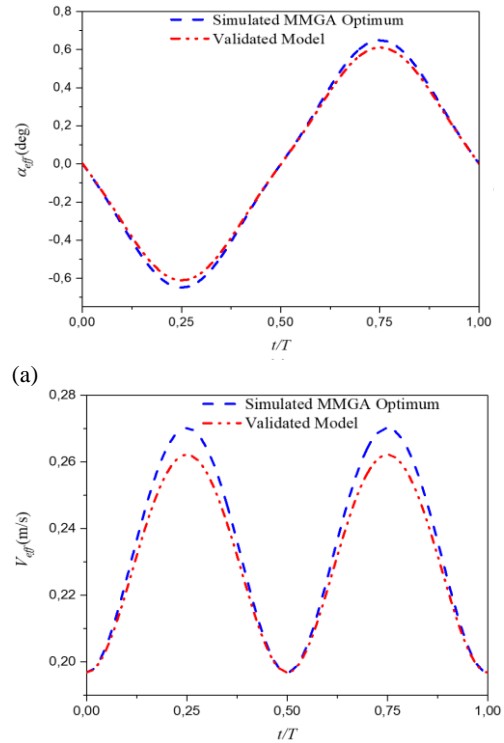


**Fig. 9. Effective angle of attack  $a_{eff}$  and effective upstream velocity  $V_{eff}$  over a flapping period of the simulated MMGA optimum versus the validated model.**

period for the two cases (case1: simulated MMGA optimum and case2: validated model against Kinsey and Dumas 2008 in section 6.1) is illustrated in Figs. 10, whose average coefficient values are summarized in Table 2 for quantitative comparison in terms of the contribution of the coefficients, namely  $Cop_h$  and  $Cop_\theta$  in the total  $Cop$  coefficient. It is important to note that both  $Cop_h$  and  $Cop_\theta$  contribute with a positive output power over the flapping cycle, where the coefficient  $Cop_h$  completely dominates in the largest part with a contribution more than 90% compared to  $Cop_\theta$ , which is insignificant for both cases. Thus, a 7.6% improvement in  $Cop_h$  using the MMGA case over the validated case leads to a 1.7% growth in the total  $Cop$ .

In order to understand better the mechanism of energy extraction performance improvement, it is worth examining the evolution of the coefficients  $C_y$ ,  $dh/dt$  and that of  $C_M$ ,  $d\theta/dt$  as given by Eq. (9). From Figs. 11, it is interesting to note that the good synchronization over the period between the lift coefficient  $C_y$ , and the heave velocity  $dh/dt$  contributes positively in the total instantaneous power coefficient  $Cop$  over the period with 98.2% and 92.8% for case1 and case2 respectively. The significant contribution of coefficients  $C_y$  and  $dh/dt$  for the first case due to the larger  $C_y$  in the region of the peaks and near them for the MMGA case is compared to that of the validated model. Regarding the contribution of the coefficients  $C_M$ ,  $d\theta/dt$  shown in Fig. 11(b), the period has been divided into time intervals "A" to "H". It can be clearly seen that the good synchronization of the aforementioned

**Table 2 Time-averaged power coefficient,  $Cop_h$ -mean,  $Cop_\theta$ -mean and  $Cop$ -mean of case1 and case2**

	$Cop_h$ -mean	$Cop_\theta$ -mean	$Cop$ -mean
<b>Case1</b>	0,856	0,015	0,871
<b><math>Cop_h</math>-mean <math>Cop_\theta</math>-mean Contribution</b>	98,20%	1,80%	100%
<b>Case2</b>	0,795	0,062	0,856
<b><math>Cop_h</math>-mean <math>Cop_\theta</math>-mean Contribution</b>	92,80%	7,20%	100%
<b>Improvement Case1 VS Case2</b>	7.6%	-24.2%	1.7%

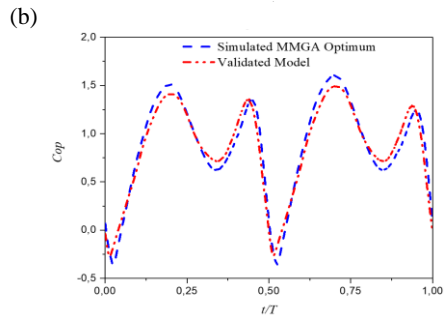
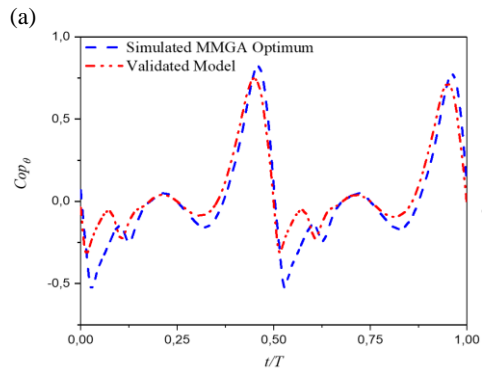
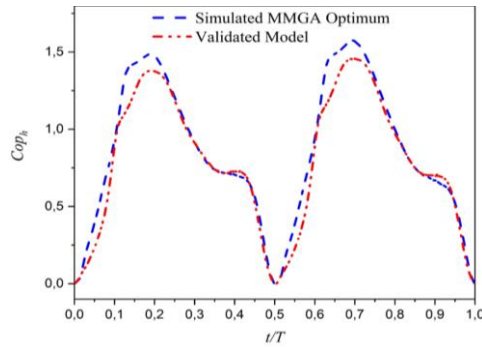


**Fig. 10. Instantaneous power coefficient  $Cop_h$ ,  $Cop_\theta$  and  $Cop$  over a flapping period of case1 versus case2.**

coefficients leads to a positive contribution in time intervals B, D, F, and H, while a negative

contribution is observed in the rest of the time intervals for both cases, thus causing a minor contribution over a cycle of  $Cop_\theta$  of 1.8% and 7.2%

for case1 and case2 respectively as can be seen in Table 2.

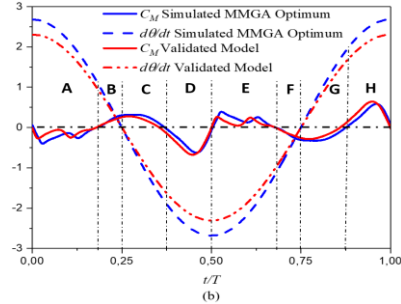
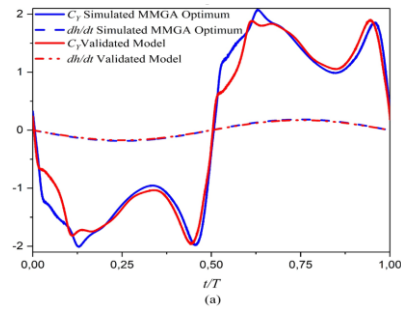


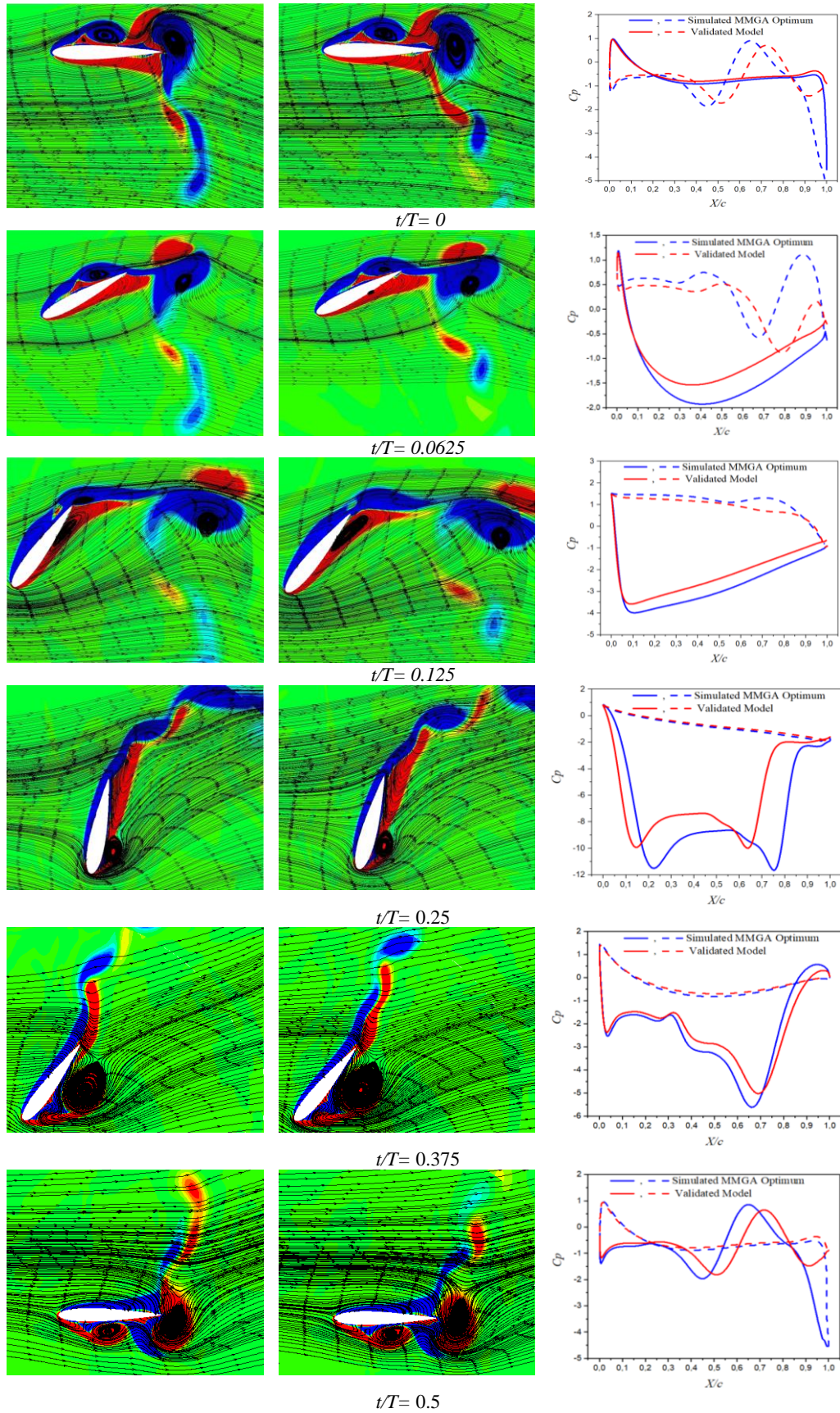
**Fig. 11. Instantaneous variation of, lift coefficient ( $C_L$ ), heave velocity ( $dh/dt$ ), moment coefficient ( $C_M$ ) and pitch velocity ( $d\theta/dt$ ) over one flapping period for the compared cases.**

The variation of the coefficient  $C_L$  during a flapping cycle affects the power extracted from the fluid. The values of  $C_L$  is influenced by the flow fields and pressure coefficient distributions around the wing. Hence, it is needed to examine carefully the flow fields and the pressure coefficient distributions in order to understand better the improvement of the power extraction process.

In view of the enhancement of the coefficient  $C_L$  (see Figs. 11(a)) in the interval time  $[0, 0.2]$  that is symmetrical to that in the interval  $[0.5, 0.7]$ . The evolution of the instantaneous vortex contour and the pressure coefficient distributions at times  $t/T=0$ ,  $t/T=0.0625$ ,  $t/T=0.125$ ,  $t/T=0.25$ ,  $t/T=0.375$  and  $t/T=0.5$  around the wing of the simulated optimum and the validated model for a half period have been explored as shown in Figs. 12.

It is important to mention that the vortex contours and the pressure coefficients in the other half period are inversely symmetrical to those in this half period.

Examining the flow around the wing clarifying the vortex formation process for both studied cases is demonstrated in Figs. 12(a) and Figs. 12(b). It is remarkable that a leading edge vortex (LEV) starts its formation around the time  $t/T=0.25$  where the pitch angle and heave velocity reach their maxima. During the wing motion, the LEVS reach their extreme intensity in each half cycle just before  $t/T=0$  and  $t/T=0.5$ . Then, the LEVS interact with the rest of the wing after it projects into the wake.



(a) (b) (c)  
**Fig. 12. Instantaneous vortex contour, (a) simulated optimum MMGA, (b) validated model, (c) pressure coefficients, for both compared cases at selected times over a half-flapping period: solid and dashed lines presents lower and upper wall pressure.**

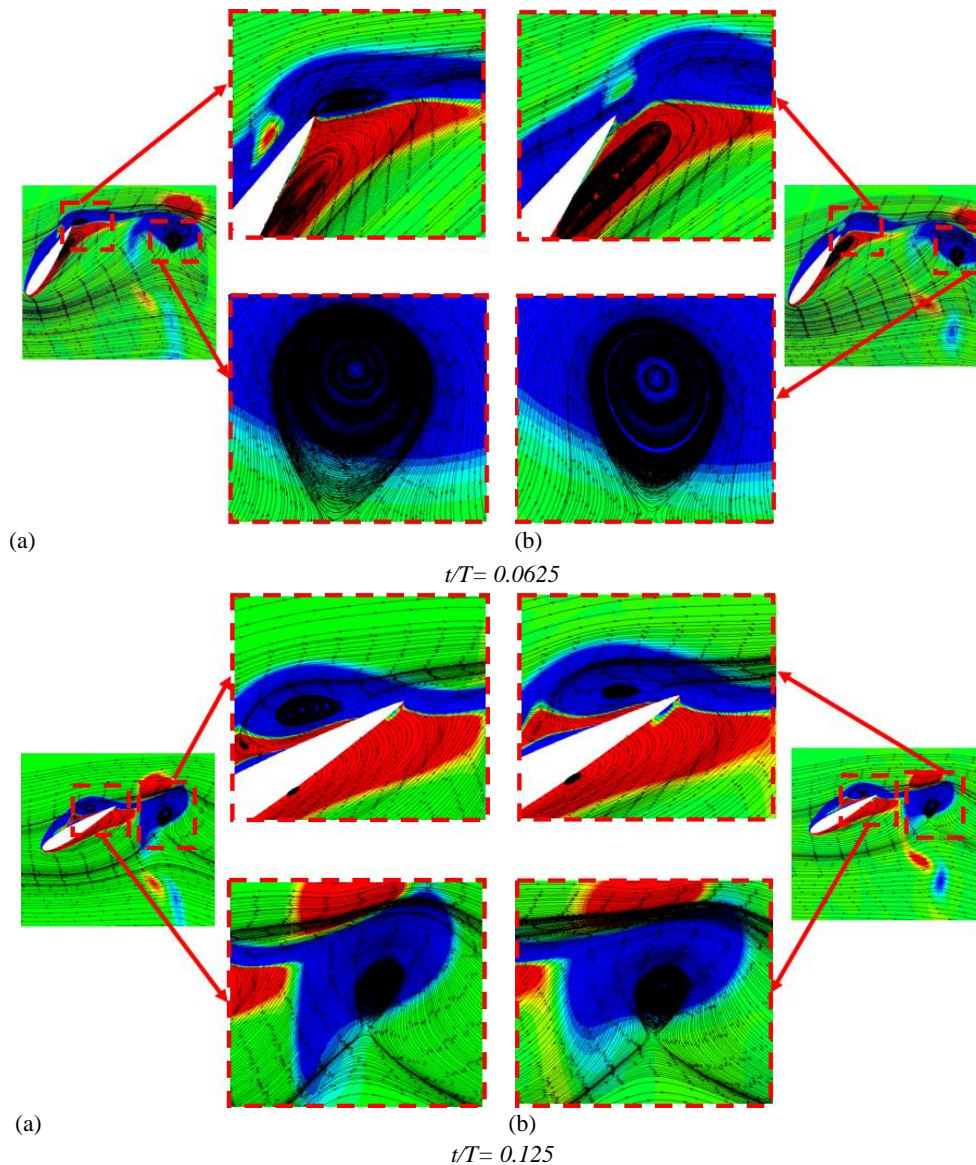


**Fig. 13. Leading edge vortex and trailing edge vortex contours at times  $t/T=0.0625$  and  $t/T=0.125$ , (a) simulated optimum MMGA, (b) validated model.**

It should be noted that the flow fields of the two studied cases are almost similar with a small difference on the LEV and TEV vortices characterized by an extension and a stretching of the trailing edge vortices for the simulated optimum compared to the validated case, which may be an indication of more intense vortices for the first case.

An in-depth analysis of the LEVS and TEVS has been performed to judge the intensity of the vortices for the two compared cases, a zoom has been completed for the instants  $t/T=0.0625$  and  $t/T=0.125$  from the interval time  $[0, 0.2]$  as indicated in Figs. 13. It is clearly seen that the simulated optimum LEVS and TEVS seems to be strongest than that of validated case at the selected instants due to the higher effective angle of attack and larger effective upstream velocity, which, on the one hand, results in an increase of the effective dynamic pressure and consequently the lift force, on the other hand favors

a strongest dynamic-stall vortex shedding improving the efficiency of energy extraction for the simulated optimum.

Figures 12(c) displays that the range of pressure difference distribution between the upper and the lower wing surfaces is greater for the simulated optimal case, leading to an augmentation in the lift force at the instants  $t/T=0.125$  and  $t/T=0.625$  according to the Fig. 11(a).

### 6.2.6 Efficiency Response Surface and Factors Interaction

The presented blue points in Figs. 14, Figs. 15 and Figs. 16 are the responses (efficiencies) of the 13 Box-Behnken variants obtained from the simulation. The 3D response surface represents the predicted efficiency using RSM that contains the optimum

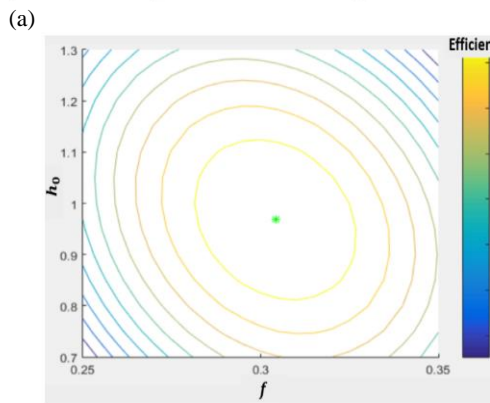
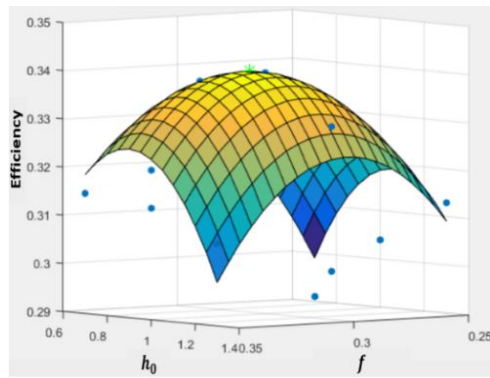


**Fig. 14. (a) Response surface for the predicted efficiency, (b) contour plot according to  $h_0$  and  $f$ .**

mentioned with the green star. The optimal configuration that maximizes energy extraction efficiency to 34.02 %, is located at a dimensionless heaving amplitude of 0.968, a high pitch amplitude of 1.404 radian (80.44 degrees), and a low flapping frequency of 0.304Hz.

The constructed response surface and contour lines including the optimum are represented in Figs. 14. These data reflect the effect of the dimensionless heaving amplitude  $h_0$  and the flapping frequency  $f$  on the efficiency at the optimal pitching amplitude of 1.404 radian (80.44°). The obtained results reveal that on the one hand fixing frequency at 0.25 hertz and increasing  $h_0$  to reach 0.968 improve the energy extraction efficiency from 0.3 to 0.32. On the other hand, the efficiency decreases to a value of 0.31 for  $h_0$  varying from 0.968 to 1.3. A similar trend is reached when the frequency has been fixed at 0.35. The efficiency has been improved slightly from 0.318 to 0.325 for an  $h_0$  varying from 0.7 to 0.968 then the efficiency gradually decreases to 0.302. However, increasing the frequency from 0.25 to 0.304 hertz strongly contributes to improve the efficiency from 0.297 to 0.325 for  $h_0$  fixed at 0.7. This contribution decreases with frequencies differed from 0.304 to 0.35 and the predicted efficiency reaches 0.318, while for  $h_0$  is held at 1.3. The efficiency is improved from 0.31 to 0.325 with frequency ranging from 0.25 to 0.304. This trend is reversed, and the efficiency strongly decreases from 0.325 to 0.302 for a changing frequency between 0.304 and 0.35. The significant quasi-symmetrical quadratic effect of both factors, i.e.  $h_0$  and  $f$  on the

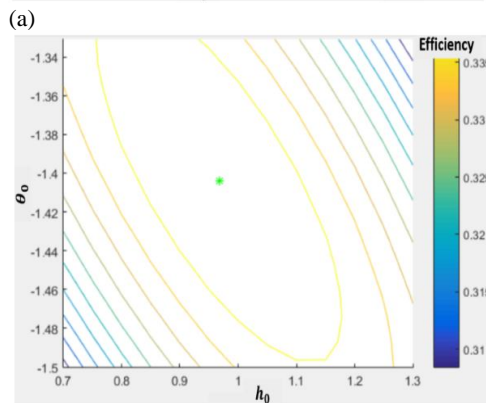
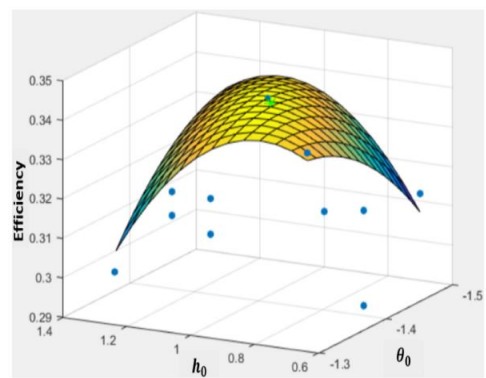


**Fig. 15. (a) Response surface for the predicted efficiency, (b) contour plot according to  $h_0$  and  $\theta_0$ .**

predicted efficiency shape leads to parabolic response surface. These effects can be clearly observed from the contour map lines.

Figures 15 show the response surface and the map contours line versus the dimensionless heaving amplitude  $h_0$  and pitching amplitude  $\theta_0$ , where the frequency is fixed on the optimal value of 1.404 radian (80.44°). By one way, while increasing  $h_0$  from 0.7 to 0.968 with  $\theta_0$  fixed on 1.33 the efficiency increases slightly from 0.337 to 0.34 after that it strongly decreases down to 0.31. However, increasing  $h_0$  from 0.7 to 1.15 with  $\theta_0$  fixed on 1.5 strongly increases the efficiency from 0.307 to 0.337. After that, it slightly decreases to 0.333 when increasing  $h_0$  from 1.15 to 1.3. On the other hand, increasing  $\theta_0$  from 1.33 to 1.5 with  $h_0$  fixed on 1.3 progressively augments the efficiency from 0.308 to 0.333, but increasing  $\theta_0$  from 1.33 to 1.5 with  $h_0$  fixed on 0.7 leads to decrease gradually the efficiency from 0.336 to 0.307. In addition, the interaction between the factors  $h_0$  and  $\theta_0$  is greater for a high  $h_0$  and low  $\theta_0$  or the opposite. Concerning the quadratic effect between the factors leads to diagonal elliptical parabolic illustrated from the line contours. From the contour maps, it is remarkable that the optimal efficiency is detected on the interval major part of  $\theta_0$ .

In Figs. 16, the factors effect, the frequency  $f$  and the pitching the amplitude  $\theta_0$  are quantified with dimensionless heaving amplitude fixed on the optimal value of 0.968. A paraboloid surface is obtained due to the strong quadratic effect of the

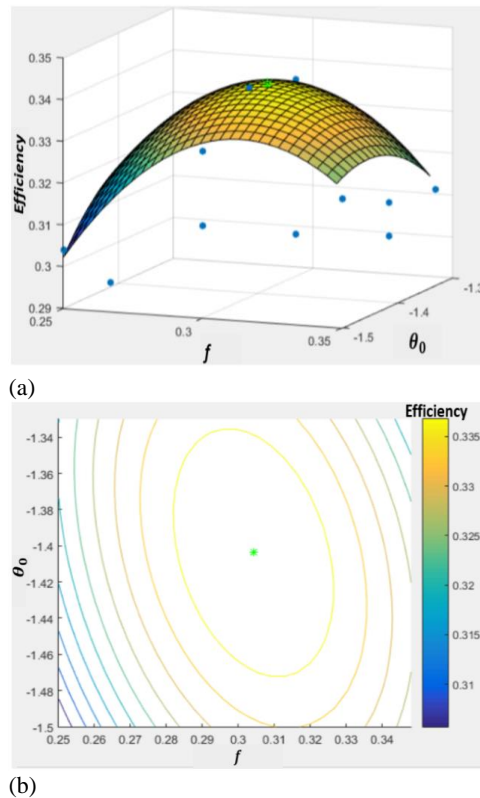


**Fig. 16. (a) Response surface for the predicted efficiency, (b) contour plot according to  $\theta_0$  and  $f$ .**

frequency  $f$ . The interaction effect between the factors manifests and leads to the following effects: (1) the increase of  $\theta_0$  conducts to an efficiency improvement from 0.304 to 0.319 particularly for  $f$  under 0.28 hertz; (2) for higher values of  $f$  ( $>0.32$ ) the increase of  $\theta_0$  conducts to a moderate efficiency decrease from 0.325 to 0.315.

## 6. CONCLUSION

The objective of this numerical study is to predict and maximize the efficiency of NACA 0015 fully activated flapping airfoil using the response surface method and genetic algorithms. 2-D numerical computations have been carried out to quantify the performances and to calculate the aerodynamic forces of the flapping airfoil. Relying on the response surface methodology and Genetic algorithms has made it possible to achieve an energy extraction efficiency of 34.02% with an inexpensive simulation cost with the optimal configuration of kinematic parameters of a dimensionless heaving amplitude of 0.968, a high pitching amplitude of 80.44 degrees, and a low flapping frequency of 0.304 hertz. The predicted response surface based on the quadratic polynomial approximation while utilizing MMGA has anticipated the simulated efficiencies with adequate statistical estimators. The obtained results reveal that:

1. The heave motion fully dominates the energy extraction process compared to the pitch motion with a positive contribution in the total power of 98.2%.

2. A maximum effective angle of attack of  $37.24^\circ$  seems to dominate kinematic factor, leading to the enhancement of the energy extraction efficiency.
3. The quadratic quasi-symmetrical effect of both factors  $h_0$  and  $f$  is significant, and it leads to a parabolic response surface.
4. The interaction between the factors  $h_0$  and  $\theta_0$  is greater for a high  $h_0$  and low  $\theta_0$ , where the quadratic effect between the factors leads to an elliptical paraboloid.
5. The interaction effect between the factors  $f$  and  $\theta_0$  is significant but the quadratic effect of the frequency is strong.

This work is a platform for future contributions where a fully automated multi-objective method based on a radial basis function response surface coupled to NSGAI (RBF- NSGAI) is being developed. The objective of this method is to detect the optimal configuration of a large number of kinematic parameters by using a non-sinusoidal flapping trajectory, in order to maximize the performance of energy extraction from a flapping wing. In addition, a comparative study between the MMGA optimization methods used in this study and RBF-NSGAI is done in terms of optimization solutions and method performance. Furthermore, the effect of kinematic parameters and the interaction between them as well as the contribution of these parameters in the energy extraction performance are investigated.

## ACKNOWLEDGEMENTS

The IUSTI laboratory Aix-Marseille University was part of this research, we express our gratitude for Professor Marc MEDALE for his continuous encouragement during the achievement of this work. We express our sincere thanks to the laboratory staff for the programming learning opportunities.

## REFERENCES

- Anderson, J. M., K. Streitlien, D. S. Barrett and M. S. Triantafyllou (1998). Oscillating foils of high propulsive efficiency. *Journal of Fluid Mechanics* 360, 41-72.
- Betiku, E., V. O. Odude, N. B. Ishola, A. Bamimore, A. S. Osunleke and A. A. Okeleye (2016). Predictive capability evaluation of RSM, ANFIS and ANN : A case of reduction of high free fatty acid of palm kernel oil via esterification process. *Energy Conversion and Management* 124, 219-230.
- Boudis, A., H. Oualli, A. Benzaoui, O. Guerri, A. C. Bayeul-Lainé and O. Coutier-Delgosha (2021). Effects of non-sinusoidal motion and effective angle of attack on energy extraction performance of a fully activated flapping foil. *Journal of Applied Fluid Mechanics* 14(2), 485-498.
- Box, G. E. P. and D. W. Behnken (1960). Some new

- three level desing for study of quantitative variables box. *Technometrics* 2(4), 455-475.
- Dharma, S. M. H. H., H. H. Masjuki, H. C. Ong, A. H. Sebayang, A. S. Silitonga, F. Kusumo and T. M. I. Mahlia (2016). Optimization of biodiesel production process for mixed *Jatropha curcas* – *Ceiba pentandra* biodiesel using response surface methodology. *Energy Conversion and Management* 115,178-190.
- Goldberg, D. E. (2000). The Design of Innovation: Lessons from and for Competent Genetic Algorithms. *Technological Forecasting & Social Change* 64(1), 7-12.
- Haftka, R. T. (1996). Response surface approximations for structural optimization W. J. Roux AIAA, NASA, and ISSMO. In *Symposium on Multidisciplinary Analysis and Optimization*.
- Holland, J. H. (1992). Genetic Algorithms. *Scientific American*. 267(1), 66-73.
- Ji, T., F. Jin, F. Xie, H. Zheng, X. Zhang and Y. Zheng (2022). Active learning of tandem flapping wings at optimizing propulsion performance. *Physics of Fluids* 34, 047117.
- Kinsey, T. and G. Dumas (2008). Parametric study of an oscillating airfoil in a power-extraction regime. *AIAA Journal* 46(6), 1318-1330.
- Li, Y., T. Liu, Y. Wang and Y. Xie (2022). Deep learning based real-time energy extraction system modeling for flapping foil. *Energy* 246, 123390.
- Liu, Z., K. S. Bhattacharjee, F. Tian, J. Young, T. Ray and J. C. S. Lai (2018). Kinematic optimization of a flapping foil power generator using a multi-fidelity evolutionary algorithm. *Renewable Energy* 132, 543-557.
- Ma, P., Y. Wang, Y. Xie and J. Zhang (2018). Analysis of a hydraulic coupling system for dual oscillating foils with a parallel configuration. *Energy* 143, 273–283.
- McKinney, W. and J. DeLaurier (1980). Wingmill: an oscillating-wing windmill. *J. Energy* 5(2), 109-115.
- Myers, R. H., D. C. Montgomery, G. Geoffrey Vining, C. M. Borror and S. M. Kowalski (2004). Response surface methodology: a retrospective and literature survey. *Journal of Quality Technology* 36(1), 53-78.
- Park, H. S. and X. P. Dang (2010). Structural optimization based on CADCAE integration and metamodeling techniques. *Computer-Aided Design* 42(10), 889-902.
- Platzer, M. F., M. A. Ashraf, J. Young and J. Lai (January 2009). Development of a New Oscillating-Wing Wind and Hydropower Generator, AIAA -1211. *47th AIAA Aerospace Sciences Meeting including The New Horizons Forum and Aerospace Exposition*.
- Shukla, L. and A. Nishkam (2014). Performance optimization, prediction, and adequacy by response surfaces methodology with allusion to drf technic. *International Scholarly Research Notices Text* 1-12.
- Xiao, Q., W. Liao, S. Yang and Y. Peng (2012). How motion trajectory affects energy extraction performance of a biomimic energy generator with an oscillating foil. *Renew Energy* 37(1), 61-75.
- Xu, B., Q. Ma and D Huang (2021). Research on energy harvesting properties of a diffuser-augmented flapping wing. *Renew. Energy* 180, 271-280.
- Zheng, H., F. Xie, T. Ji, Z. Zhu and Y. Zheng (2020a). Multifidelity kinematic parameter optimization of a flapping airfoil. *Physical Review E* 101, 013107.
- Zheng, H., F. Xie, T. Ji and Y. Zheng (2020b). Kinematic parameter optimization of a flapping ellipsoid wing based on the datainformed self-adaptive quasi-steady model. *Physics of Fluids* 32, 041904.
- Zhu, B. (2019). Energy extraction properties of a flapping wing with an arc-deformable airfoil. *Journal of Renewable Sustainable Energy* 11, 023302.
- Zhu, B., Y. Huang and Y. Zhang (2018). Energy harvesting properties of a flapping wing with an adaptive Gurney flap. *Energy* 152, 119-128.
- Zhu, J. and T. Tian (2017). The time asymmetric pitching effects on the energy extraction performance of a semi-active flapping wing power generator. *European Journal of Mechanics -B/Fluids* 66, 92-101.